This article has been accepted for publication in IEEE Antennas and Wireless Propagation Letters. This is the author's version which has not been fully edited and content may change prior to final publication. Citation information: DOI 10.1109/LAWP.2022.3206913

Polarization Converting Metasurface Inspired Dual Band Dual Circularly Polarized Monopole Antennas for OFF Body Communications

Nibash Kumar Sahu, Student Member, IEEE, and Sanjeev Kumar Mishra, Senior Member, IEEE

***Abstract*—This letter investigates a novel technique to achieve circular polarizations (CP) at 2.45 GHz ISM and 3.5 GHz WiMAX-bands. The behaviour is achieved by incidenting an x-polarized wave from a monopole antenna (MA) on a polarization-converting metasurface (PCMS). The PCMS operates in TM_{10} and TM_{20} modes that generate dual frequency bands and reflect a 90^0 phase-shifted y-polarized wave that, when combined with the 0^0 phase containing x-polarized wave, generates CP. To attain four separate combinations of phase-shift in terms of $+90^0$ and -90^0 in dual-bands, four distinct 2×2 PCMSs are designed, which are designated as MS_1, MS_2, MS_3, and MS_4. The MS_1-based MA (A_1) produces left-hand CP (LHCP), whereas the MS_2-based MA (A_2) produces right-hand CP (RHCP) in both frequency bands. On the other hand, the MS_3-based MA (A_3) produces RHCP in the lower-band (LB) and LHCP in the higher-band (HB), whereas the MS_4-based MA (A_4) produces LHCP in the LB and RHCP in the HB. A_3 is fabricated and measured, and the results are very close to the simulations. Each antenna has a wide impedance bandwidth, a high gain, and high efficiency with a low SAR in the desired bands, which justifies their suitability for off-body communication.**

***Index Terms*—Circular polarization, dual-band, polarization converting metasurface, OFF body communication.**

I. Introduction

In the current era of OFF-body communications, the use of the metasurface beneath the monopole antenna has grown rapidly for back radiation minimization [1-17]. The minimization of back radiation makes the radiation pattern unidirectional and, most importantly, reduces the specific absorption rate (SAR) to a safe value, which makes the antenna a suitable candidate for off-body communication. In [2–11], the development of single-band resonated antennas has been emphasized, whereas in [12–17], the development of dual-band resonated antennas has been emphasized. In the aforementioned literature, metasurfaces have been solely utilized to reduce the back-radiation. Prior to that, in [18], a mushroom-type electromagnetic band gap (EBG) structure was proposed, which not only reduces the back-radiation but also generates dual-band. However, the mushroom type EBG makes use of metallic vias, which may add design complexity. Additionally, the linearly polarized waves generated by the aforementioned literature [2–18] may result in losses such as polarization mismatch. To address the issues, dual-band dual-polarized antennas using via-free metasurfaces have been proposed [19], where the metasurface generates dual-band and reduces back radiation. However, a dual-band dual-polarized antenna generates CP only in one band and linear polarization (LP) in the other band. Prior to that, dual-bands with dual CP characteristics have been achieved using a polarization rotation metasurface based monopole antenna in [20], in which the metasurface generated CP and reduced back-radiation, whereas the MA generated dual frequency bands. However, the geometry in [20] was quite complex. Thus, there is a requirement for via-free metasurfaces with compact and simple geometry that would be able to generate dual-band with dual CP characteristics as well as reduce the back radiation.

This work presents polarization converting metasurface-inspired monopole antennas where the via-free metasurfaces generate dual frequency bands with dual CP characteristics and also reduce the back-radiation. The uniqueness of the proposed designs includes its (i) simple and novel geometry, and (ii) the attainment of various polarization states by suitably controlling the leading and lagging of the phase of reflected waves from the metasurface. The paper is divided into the following sections: Section II describes the working principle and designs of antennas; Section III discusses the FS and OB performance; and Section IV presents experimental validation followed by conclusion.

II. Working principle and design of antennas

The working principle is based on the incident of the x-polarized wave from the MA on PCMS. The PCMS is operated in TM_{10} and TM_{20} modes that generate dual frequency bands and reflect a 90^0 phase-shifted y-polarized wave, as illustrated in Fig. 1(a), that when combined with the 0^0 phase containing x-polarized wave, generates CP. To have a thorough understanding of the CP mechanism, the time harmonic far-field electric field in z-direction is formulated as follows:

$$\overrightarrow{E} = (\widehat{a}_x E_x^{um} + \widehat{a}_y R_{yx} e^{j\theta_{yx}} E_x^{dm}) e^{j(wt - k_0 z)} \quad (1)$$

Where E_x^{um} and E_x^{dm} denote the electric field components of the up-ward and down-ward directed x-polarized wave radiated from MA, respectively. R_{yx} and θ_{yx} denote the magnitude and phase of the cross-polarized reflection coefficient of the metasurface for the x-polarized wave incidence, respectively. Thus, by approaching the above principle, the design of antennas takes place using the following three steps: Step I, Step II, and Step III. In Step I, a conventional square unit-cell designated as UC, as depicted in Fig. 1(b), is theoretically

N. K. Sahu, and S. K. Mishra are with the International Institute of Information and Technology, Odisha, India-751003.
*Corresponding author e-mail: sanjeev@iiit-bh.ac.in.

© 2022 IEEE. Personal use is permitted, but republication/redistribution requires IEEE permission. See https://www.ieee.org/publications/rights/index.html for more information.
Authorized licensed use limited to: International Institute of Information Technology Bhubaneswar. Downloaded on December 16,2022 at 11:24:58 UTC from IEEE Xplore. Restrictions apply.

This article has been accepted for publication in IEEE Antennas and Wireless Propagation Letters. This is the author's version which has not been fully edited and content may change prior to final publication. Citation information: DOI 10.1109/LAWP.2022.3206913

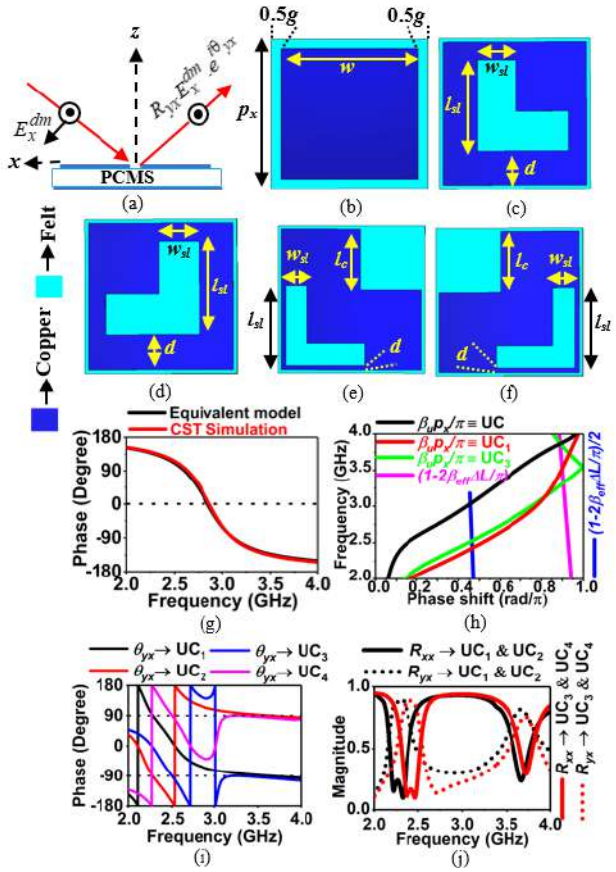

Fig. 1. (a) Polarization conversion mechanism, (b) Geometry of UC, (c) Geometry of UC_1, (d) Geometry of UC_2, (e) Geometry of UC_3, (f) Geometry of UC_4, (g) Reflection phase of UC extracted from equivalent model and simulation, (h) Dispersion characteristics of UC, UC_1, and UC_3 (i) Cross-polarized phase (θ_{yx}) curves of optimized unit-cells, and (j) Co-polarized (R_{xx}) and cross-polarized (R_{yx}) magnitude curves of optimized unit-cells.

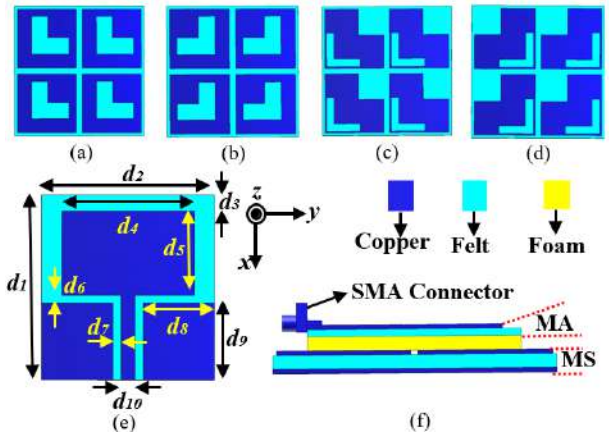

Fig. 2. Geometry of (a) MS_1, (b) MS_2, (c) MS_3, (d) MS_4, (e) MA, and (f) Metasurface (MS) based monopole antennas (MA).

designed to resonate at 3 GHz using the transmission line approach reported in [19]. First, the dielectric slab inductance (L_d) and grid capacitance (C_g) are calculated as 3.76 nH and 0.83 pF, respectively, for the substrate thickness of 3 mm. Then, the parameter 'w' is determined as nearly 29 mm for the chosen gap (g) between the unit-cells as 1.5 mm. After

TABLE I
θ_{yx} OF OPTIMIZED UNIT-CELLS WITH RESULTED STATE OF POLARIZATION

Unit-cell	θ_{yx} at 2.4 / 3.6 GHz	Unit-cell based antenna	Polarization at 2.4 / 3.6 GHz
UC_1	$+90^0$ / -90^0	A_1	LHCP/LHCP
UC_2	-90^0 / $+90^0$	A_2	RHCP/RHCP
UC_3	-90^0 / -90^0	A_3	RHCP/LHCP
UC_4	$+90^0$ / $+90^0$	A_4	LHCP/RHCP

that, the theoretically developed UC is simulated using CST software by taking the felt substrate of ε_r = 1.6 and $\tan\,\delta$ = 0.044. Fig. 1(g) shows the theoretical and simulated phases of reflection coefficients, which indicate a good match with each other with a 0^0 reflection phase at 3 GHz. To determine the associated frequency for TM_{10} and TM_{20} modes of operation, the dispersion characteristic is depicted in Fig. 1 (h) for the 2×2 configurations of UC, which is extracted using MATLAB software by approaching the following reproduced equations [19]:

$$\frac{\beta_u p_x}{\pi} = \frac{1 - 2\beta_{eff}\Delta L/\pi}{2}, for TM_{10} mode \tag{2}$$

$$\frac{\beta_u p_x}{\pi} = 1 - 2\beta_{eff}\Delta L/\pi, for TM_{20} mode \tag{3}$$

$$\beta_u p_x = \cos^{-1}\left(\frac{1 - S_{11}S_{22} + S_{12}S_{21}}{2S_{21}}\right) \tag{4}$$

Where, β_u denotes the propagation constant of the unit cell, and p_x denotes the period along the x-direction. The dispersion characteristic shows that TM_{10} is generating at 3 GHz and the TM_{20} mode is generating at 3.9 GHz.

In Step II, the UC is modified to lower the associated frequency of operating modes towards the required bands and to obtain y-polarized reflected wave with phase (θ_{yx}) of ±90^0. Since the +90^0 and -90^0 in the LB and HB can happen in four combinations. To attain all of these combinations, four different polarization converting unit cells UC_1, UC_2, UC_3, and UC_4 are optimized from UC as shown in Fig. 1(c), (d), (e), and (f), respectively. The dimensions of UC_1 and UC_2 are as follows: w = 29 mm, g = 1.5 mm, l_{sl} = 18.5 mm, w_{sl} = 8 mm, and d = 7.6 mm. The dimensions of UC_3 and UC_4 are as follows: w = 32 mm, g = 1.5 mm, l_{sl} = 18 mm, w_{sl} = 5 mm, l_c = 14 mm, and d = 15 mm. Fig. 1 (i) depicts the cross-polarized phase curves of all the optimised unit-cells, and their resultant values at 2.4 GHz and 3.6 GHz are summarised in Table I. An abrupt jump of phases is seen at nearly 3 GHz in the curve of UC_3 due to the phase wrapping [21]. Fig. 1 (j) depicts the R_{xx} and R_{yx} curves of all the optimized unit-cells, revealing the strong x-to-y polarization convertions in both the bands. The dispersion characteristics of UC_1 (≡UC_2) and UC_3 (≡UC_4) for their 2×2 configurations are illustrated in Fig. 1(h), which reveals that the TM_{10} and TM_{20} modes are generated at nearly 2.4 GHz and 3.5 GHz, respectively.

In step-3, UC_1, UC_2, UC_3, and UC_4 are arranged into 2×2 configuration, which results in the metasurface of MS_1, MS_2, MS_3, and MS_4, respectively, as shown in Fig. 2 (a-d). Then, to excites these metasurfaces, a CPW-fed MA is designed using 1.5 mm of felt substrate with ε_r = 1.6 and $\tan\,\delta$ = 0.044 for

© 2022 IEEE. Personal use is permitted, but republication/redistribution requires IEEE permission. See https://www.ieee.org/publications/rights/index.html for more information.
Authorized licensed use limited to: International Institute of Information Technology Bhubaneswar. Downloaded on December 16,2022 at 11:24:58 UTC from IEEE Xplore. Restrictions apply.

This article has been accepted for publication in IEEE Antennas and Wireless Propagation Letters. This is the author's version which has not been fully edited and content may change prior to final publication. Citation information: DOI 10.1109/LAWP.2022.3206913

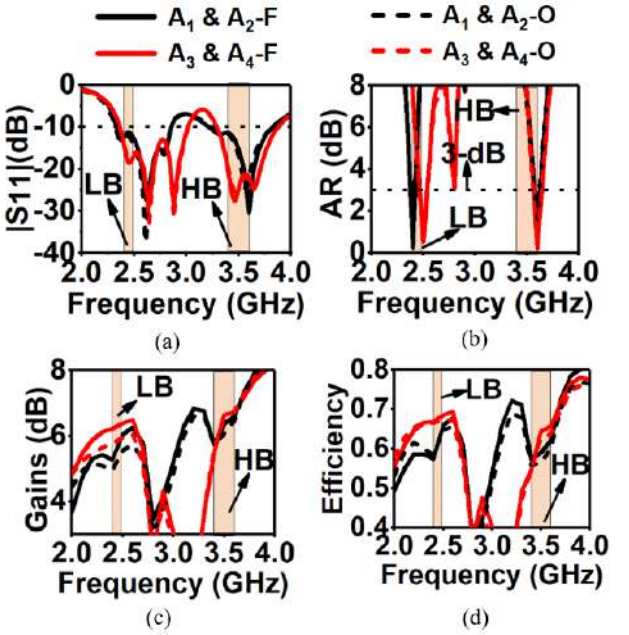

Fig. 3. Simulated free space (F) and on-body (O) performances (a) Reflection coefficients, (b) AR, (c) Gain, and (d) Efficiencies.

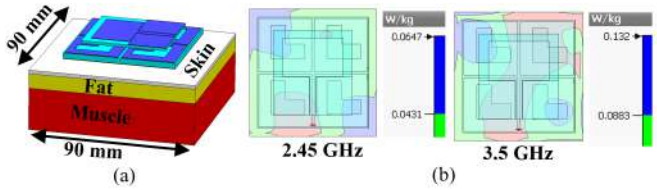

Fig. 4. (a) Geometry of the body-model, and (b) SAR obtained by A_1.

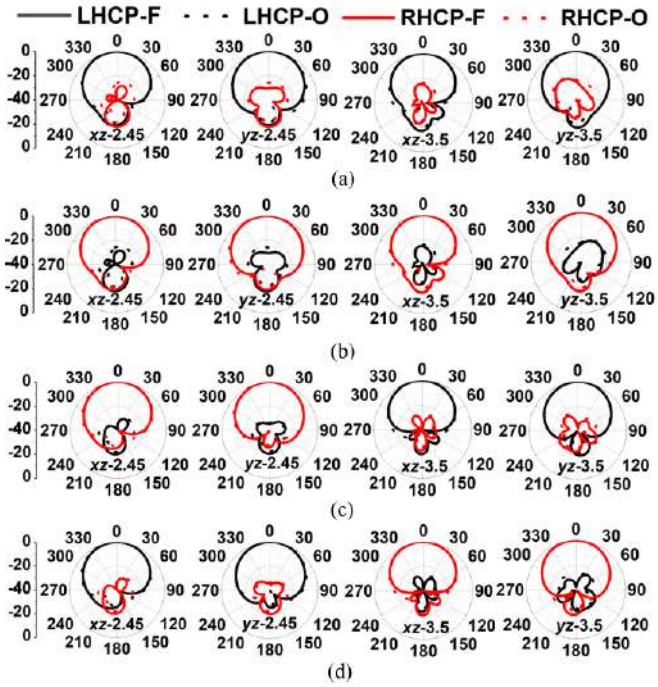

Fig. 5. Simulated FS (F) and OB (O) LHCP and RHCP in xz and yz-planes at 2.4 GHz and 3.6 GHz for (a) A_1 (b) A_2 (c) A_3, and (d) A_4.

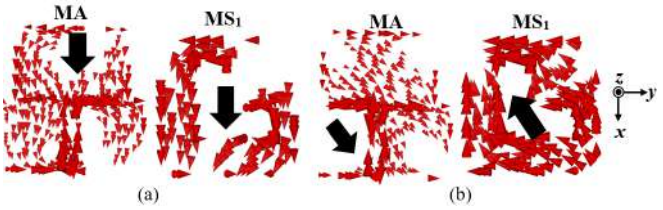

Fig. 6. Surface current distribution on the MA and one of the unit-cell of MS_1 at (a) 2.4 GHz, and (b) 3.6 GHz.

TABLE II
ANTENNA PERFORMANCES

Structure	BW (MHz) F/O	Effic-iency F/O	Gain (dBi) F/O	AR-BW (MHz) F/O	SAR in W/Kg
A_1(LB)	530/540	0.7/0.7	6.3/5.8	70/70	0.06
A_1(HB)	620/580	0.8/0.8	7.9/8	90/90	0.1
A_2(LB)	530/540	0.7/0.7	6.3/5.8	70/70	0.06
A_2(HB)	620/580	0.8/0.8	7.9/8	90/90	0.1
A_3(LB)	640/660	0.7/0.7	6.5/6.1	70/70	0.04
A_3(HB)	600/590	0.8/0.8	7.8/7.8	100/100	0.06
A_4(LB)	640/660	0.7/0.7	6.5/6.1	70/70	0.04
A_4(HB)	600/590	0.8/0.8	7.8/7.8	100/100	0.06
M.A_3(LB)	510/470	NA	6	65	NA
M.A_3(HB)	560/520	NA	7	90	NA

M.:Measured, F: Free-space, O:On body, and NA: Not acceptable.

resonating at 3 GHz, as shown in Fig. 2(e). The dimensions of MA are as follows: d_1 = 45 mm, d_2 = 42 mm, d_3 = 4 mm, d_4= 33 mm, d_5 = 21 mm, d_6 = 0.4 mm, d_7 = 0.32 mm, d_8 = 18.93 mm, d_9 = 19.60 mm, and d_{10} = 3.5 mm. Fig. 2(f) shows the geometry of the stacking of the MA on the metasurface. The stacking of the MA on MS_1, MS_2, MS_3, and MS_4 is designated as antenna A_1, A_2, A_3, and A_4, respectively.

III. FREE SPACE AND ON-BODY PERFORMANCES

Fig. 3 shows the FS and OB performances of each antenna, including reflection coefficient (S_{11}), axial ratio (AR), realized gain, and radiation efficiency, with summaries of results in Table II. The OB performances are carried out by placing all the antennas at a 3 mm distance on a rectangular body model as shown in Fig. 4 (a). The body model is made of skin, fat, and muscle layers with the same thickness and electrical properties as described in [2]. Fig. 4 (b) illustrate the 10 g standard SAR distributions for A_1 at 2.45 GHz and 3.5 GHz with 0.1 W of input power. In the same way, the SAR distributions of the other antennas are evaluated and summarized in Table II.

In order to determine the behaviour of the polarizations of the radiated waves from the antennas, the LHCP and RHCP patterns as shown in Fig. 5 are produced. When the strength of the RHCP pattern is stronger than the LHCP pattern, it is considered the RHCP state of polarization and vice-versa for the LHCP state of polarization. The resultant polarization states are summarized in Table I. The obtained polarizations can be validated theoretically by drawing the tip of the electric field formulated in (1) for the progression of 'wt' from 0^0 to 180^0 with a fixed value of θ_{yx}. For example, at 2.4 GHz, the surface current distributions on the MS of A_1 are parallel with

© 2022 IEEE. Personal use is permitted, but republication/redistribution requires IEEE permission. See https://www.ieee.org/publications/rights/index.html for more information.
Authorized licensed use limited to: International Institute of Information Technology Bhubaneswar. Downloaded on December 16,2022 at 11:24:58 UTC from IEEE Xplore. Restrictions apply.

This article has been accepted for publication in IEEE Antennas and Wireless Propagation Letters. This is the author's version which has not been fully edited and content may change prior to final publication. Citation information: DOI 10.1109/LAWP.2022.3206913

TABLE III
COMPARISON OF PROPOSED WORKS WITH PREVIOUS WORKS

Reference	Freq. (GHz)	BW (%)	Gain (dB)	Efficiency	No. of unit-cells	Footprints (λ_g^2)	Use of Metasurface	Polarizations
[12]	3.5/5.8	5/7.4	9.07/7.66	0.83/0.91	4×4	3.06 @ 3.5 GHz	MB	LP/LP
[13]	2.45/5.5	12/16.3	2.5/0 4	0.4/0.4	4×4	0.87@ 2.45 GHz	MB	LP/LP
[14]	2.45/5.8	4/12	6.4/7.6	-	3×3	1.33 @ 2.45GHz	MB	LP/LP
[15]	1.8/2.45	10.9/5.1	1∼2	-	3×3	1.38 @ 1.8 GHz	MB	LP/LP
[18]	2.45/3.65	15.7/2.3	4.25/7.35	0.97/0.88	3×3	0.53 @ 2.45GHz	MB and GD	LP/LP
[19] (A_2)	2.45/3.5	14.3/12.8	6.4/8.2	0.7/0.84	2×2	0.38 @ 2.45GHz	MB and GD	RHCP/LP
[19] (A_4)	2.45/3.5	8.5/23.8	6.1/8.3	0.7/0.85	2×2	0.38 @ 2.45GHz	MB and GD	LP/RHCP
[20] (P-I)	3.5/5.8	11.7/9.1	6.6/7.2	0.57/0.6	3×3	0.64 @ 3.5GHz	MB and GC	LHCP/RHCP
[20] (P-II)	3.5/5.8	11.7/7.2	5.9/6	0.47/0.5	3×3	0.64@3.5GHz	MB and GC	LHCP/RHCP
Proposed A_1	2.45/3.5	20.5/17.7	6.3/7.9	0.7/0.8	2×2	0.39 @ 2.45GHz	MB, GD and GC	LHCP/LHCP
Proposed A_2	2.45/3.5	20.5/17.7	6.3/7.9	0.7/0.8	2×2	0.39 @ 2.45GHz	MB, GD and GC	RHCP/RHCP
Proposed A_3	2.45/3.5	24/16.8	6.5/7.8	0.7/0.8	2×2	0.47 @ 2.45GHz	MB, GD and GC	RHCP/LHCP
Proposed A_4	2.45/3.5	24/16.8	6.5/7.8	0.7/0.8	2×2	0.47 @ 2.45GHz	MB, GD and GC	LHCP/RHCP

No.: number, MB: Minimization of back radiation, GD: Generation of dual-band, GC: Generation of CP, and NA: Not acceptable

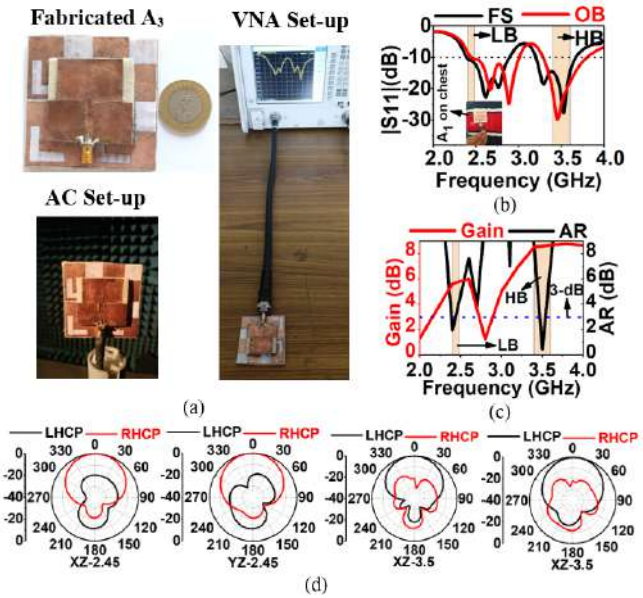

Fig. 7. (a) The schematic of the fabricated A_3, S_{11} measurement set-up using the VNA and radiation pattern measurement set-up in side the anechoic chamber (AC), (b) Measured FS and OB S_{11} with OB measurement set-up in the insert, (c) Measured FS gain and AR, (d) Measured FS LHCP and RHCP at 2.45 GHz and 3.5 GHz in the xz and yz plane.

the MA, as shown in Fig. 6(a), indicating that the reflected and direct components have the same sign [20]. Therefore, with θ_{yx} = +90^0, the tip of the total electric field is rotating in a clock-wise direction for the phase progression, which conforms to the LHCP state [22]. At 3.6 GHz, however, the surface current distributions on the MS are anti-parallel with the MA, as shown in Fig. 6(b), indicating that the reflected and direct components have the opposite sign [20]. Therefore, with θ_{yx} = -90^0, the tip of the total electric field is still rotating in a clock-wise direction for the phase progression, which conforms to the LHCP state [22].

IV. EXPERIMENTAL VALIDATION

One of the proposed structures, A_3, is fabricated and measured to validate the simulation results. Fig. 7 (a) illustrates the schematic of the fabricated structure and its FS measurement set-ups, which include a vector network analyzer (VNA) for measuring S_{11} and an anechoic chamber for measuring radiation pattern. Fig. 7 (b) illustrates the extracted results of FS and OB reflection coefficients from the VNA. To test the physical OB performance, the fabricated antenna is placed on the human chest as shown in the insert of Fig. 7 (b). The measured FS AR and gains are illustrated in Fig. 7(c). Fig. 7(d) shows the measured FS LHCP and RHCP patterns at 2.45 GHz and 3.5 GHz in the xz and yz planes. Table II summarizes all the measured results, which indicate an excellent match with the simulation results.

Table III compares the proposed work's results with the existing literature using a logical set of criteria such as impedance bandwidth, polarization, gain, and size, etc. All of the proposed antennas have better impedance bandwidth than the existing antennas. They also produce high gains, high efficiency, and CP characteristics with compact structures.

V. CONCLUSION

This paper investigated four different PCMS based MAs that are A_1, A_2, A_3, and A_4 to achieve four combination CP states in dual-bands that cover 2.45 GHz ISM-band and 3.5 GHz WiMAX-band. The PCMSs are developed by controlling the leading and lagging of the y-polarized reflected wave's phase. A_1 generates LHCP and A_2 generates RHCP in both bands. On the other hand, A_3 generates RHCP in the LB and LHCP in the HB, whereas A_4 generates LHCP in the LB and RHCP in the HB. Each antenna has a wide impedance bandwidth of more than 540 MHz, a high gain of more than 6.1 dBi, a high efficiency of more than 0.7, and a low SAR of less than 0.1 W/Kg with unidirectional radiation patterns in both bands, making them suitable for efficient OFF-body communications.

REFERENCES

[1] P. S. Hall, and Y. Hao, Antennas and propagation for body-centric wireless communications, Artech Houce, Noorwood, MA, USA,2012.

[2] M. E. Atrash, O. F. Abdalgalil, I. S. Mamoud, M. A. Abdalla, and S. R. Zahran, "Wearable high gain low SAR antenna loaded with backed all-textile EBG for WBAN applications," *IET Microw. Antennas Propag*, vol. 14, no. 8, pp. 791-799, 2020.

[3] S. M. Saeed, C. A. Balanis, C. R. Birtcher, A. C. Durgun, and H. N. Shaman, "Wearable flexible reconfigurable antenna integrated with artificial magnetic conductor," *IEEE Antennas Wireless Propag. Lett.*, vol. 16, pp. 2396-2399, 2017.

© 2022 IEEE. Personal use is permitted, but republication/redistribution requires IEEE permission. See https://www.ieee.org/publications/rights/index.html for more information.
Authorized licensed use limited to: International Institute of Information Technology Bhubaneswar. Downloaded on December 16,2022 at 11:24:58 UTC from IEEE Xplore. Restrictions apply.

This article has been accepted for publication in IEEE Antennas and Wireless Propagation Letters. This is the author's version which has not been fully edited and content may change prior to final publication. Citation information: DOI 10.1109/LAWP.2022.3206913

[4] H. R. Raad, A. I. Abbosh, H. M. Al-Rizzo, and D. G. Rucker, "Flexible and compact AMC based antenna for telemedicine applications," *IEEE Trans. Antennas Propag.*, vol. 61, no. 2, pp. 524-531, 2013.

[5] M. A. B. Abbasi, S. S. Nikolaou, M. A. Antoniades, M. N. Stevanovic, and P. Vryonides, "Compact EBG-backed planar monopole for BAN wearable applications," *IEEE Trans. Antennas Propag.*, vol. 65, no. 2, pp. 453-463, 2017.

[6] G. Goa, C. Yang, B. Hu, R. Zhang, and S. Wang, "A wearable PIFA with an all-textile metasurfaces for 5 GHz WBAN applications," *IEEE Antennas Wireless Propag. Lett.*, vol. 18, no. 2, pp. 288-292, 2019.

[7] Z. H. Jiang, D. E. Brocker, P. E. Sieber, and D. H. Werner, "A compact, low-profile metasurface-enabled antenna for wearable medical body area devices," *IEEE Trans. Antennas Propag.*, vol. 62, no. 8, pp. 4021-4030, 2014.

[8] W. Liu, Z. N. Chen and X. Qing, "Metamerial-based low profile broadband mushroom antenna," *IEEE Trans. Antennas Propag.*, vol. 62, no. 3, pp. 1165-1172, 2014.

[9] N. S. Nie, X. S. Yang, Z. N. Chen, and B. Wang, "A low-profile wideband hybrid metasurface antenna array for 5G and WiFi systems," *IEEE Trans. Antennas Propag.*, vol. 1, no. 1, pp. 1-1, 2019.

[10] T. Yue, Z. H. Jiang, and D. H. Werner, "Compact, wideband antennas enabled by interdigitated capacitor-loaded metasurfaces," *IEEE Trans. Antennas Propag.*, vol. 64, no. 5, pp. 1595-1606, 2016.

[11] G.-P. Gao, B. Hu, S.-F. Wang, and C. Yang, "wearable circular ring slot antenna with EBG structure for wireless body area network," *IEEE Antennas Wireless Propag. Lett.*, vol. 17, no. 3, pp. 434-437, 2018.

[12] M. E. Atrash, M. A. Abdalla, and M. H. Elhennawy, "A wearable dual-band low profile high gain low SAR antenna AMC-backed for WBAN application," *IEEE Trans. Antennas Propag.*, vol. 67, no. 10, pp. 6378-6388, 2019.

[13] Y. Sen, J. S. Ping, and A. E. V. Guy, "Low-profile dual-band textile antenna with artificial magnetic conductor plane," *IEEE Trans. Antennas Propag.*, vol. 62, no. 12, pp. 6487-6490, 2014.

[14] S. Zhu and R. Langley, "Dual-band wearable textile antenna on an EBG substrate," *IEEE Trans. Antennas Propag.*, vol. 57, no. 4, pp. 926-935, 2009.

[15] S. Valen, E. F. Sundarsingh, M. Kanagasabai, A. K. Sarma, C. Raviteja, R. Sivasamy, and J. K. Pakkathillam, "Dual-band EBG integrated monopole antenna deploying fractal geometry for wearable applications," *IEEE Antennas Wireless Propag. Lett.*, vol. 14, pp. 249-252, 2015.

[16] M. Wang, Z. Yang, and J. Wu, "Investigation of SAR reduction using flexible antenna with meta material structure in wireless body area network," *IEEE Trans. Antennas Propag.*, vol. 66, no. 6, pp. 3076-3086, 2018.

[17] Y. Sen, J. S. Ping, A. E. V. Guy, "Compact all-textile dual-band antenna loaded with loaded with meta material inspired structure," *IEEE Antennas Wireless Propag. Lett.*, vol. 14, pp. 1486-1489, 2015.

[18] K. Zhang, G. A. E. Vandenbosch, and S. Yan, "A novel design approach for compact wearable antennas based on metasurfaces," *IEEE Trans. Antennas Propag.*, vol. 14, no. 4, pp. 918-927, 2020.

[19] N. K. Sahu, and S. K. Mishra, "Compact dual-band dual-polarized monopole antenna using via-free metasurfaces for off body communications," *IEEE Antennas Wireless Propag. Lett.*, vol. 21, no. 7, pp. 1358-1362, 2018.

[20] H. Yang, X. Liu, Y. Fan, and L. Xiong, "Dual-band textile antenna with dual circular polarizations using polarization rotation AMC for off body communications," *IEEE Trans. Antennas Propag*, early access, Jan. 5, 2022, doi: 10.1109/TAP.2021.3138504.

[21] X. Gao, X. Han, W. P. Cao, H. F. Ma, and T. J. Cui, "Ultra-wideband and high-efficiency linear polarization converter based on double v-shaped metasurface," *IEEE Trans. Antennas Propag*, vol. 63, no. 8, pp. 3522-3530, 2015.

[22] C. A. Balanis, Antenna theory: analysis and design, 3^{rd} ed. Hoboken, NJ, USA: Wiley, 2005.

© 2022 IEEE. Personal use is permitted, but republication/redistribution requires IEEE permission. See https://www.ieee.org/publications/rights/index.html for more information.
Authorized licensed use limited to: International Institute of Information Technology Bhubaneswar. Downloaded on December 16,2022 at 11:24:58 UTC from IEEE Xplore. Restrictions apply.